Research Square

Preprints are preliminary reports that have not undergone peer review.
They should not be considered conclusive, used to inform clinical practice,
or referenced by the media as validated information.

Enhanced Prediction of Concrete Durability Using an Extended Archie's Model with a Shape Factor Approach

Hassan Parsian
Isfahan University of Technology
Davood Mostofinejad
Isfahan University of Technology
Farmehr M. Dehkordi
Polytechnic University of Turin
Farzad Naseri
farzad.naseri@studenti.polito.it

Polytechnic University of Turin

Research Article

Keywords: Electrical conductivity of concrete, Archie model, electrical resistivity of aggregates, cement paste

Posted Date: June 16th, 2026

DOI: https://doi.org/10.21203/rs.3.rs-9991010/v1

License: This work is licensed under a Creative Commons Attribution 4.0 International License.
Read Full License

Additional Declarations: No competing interests reported.

Enhanced Prediction of Concrete Durability Using an Extended Archie's Model with a Shape Factor Approach

ABSTRACT

Electrical conductivity is widely used as an indicator of concrete durability because it reflects key microstructural features such as pore network connectivity, the degree of cement hydration, and aggregate characteristics. This study presents an extended Archie's law model that explicitly incorporates aggregate shape factors and treats the cement paste as the primary conductive phase. Eighty concrete mixes with varying aggregate type (tuff and marble), gradation (Fuller curve exponents 0.20–0.65), maximum aggregate size (9.5–19 mm), and cement paste volume fraction (25–45%) were prepared and tested for electrical conductivity at 3, 7, 28, and 150 days. Results show that the extended model predicts concrete conductivity more accurately than conventional approaches, particularly at early ages, with a correlation coefficient of $R \approx 0.97$ at 3–7 days. The best-fit Archie parameters averaged $A \approx 1.54$ (tortuosity factor) and $m \approx 1.53$ (cementation exponent). Still, these coefficients evolved with curing time (e.g., A decreased from 1.81 to 1.54 while m increased from 1.43 to 1.84 over 3–150 days). Additionally, mixes with higher cement paste content exhibited higher conductivity, peaking at a paste volume of 45%. These findings highlight the significance of considering aggregate geometry and paste volume in conductivity-based durability models at early ages. However, time-dependent microstructural evolution (shape factor changes) can limit the model's predictive accuracy at later ages.

Keywords: Electrical conductivity of concrete, Archie model, electrical resistivity of aggregates, cement paste.

1. INTRODUCTION

The electrical resistivity of concrete is a key parameter used to assess its durability, as it is directly and indirectly influenced by various factors [1–3]. Incorporating durability specifications into structural design, akin to considering mechanical properties, is now widely accepted, and efforts to establish guidelines for mix designs with defined durability characteristics have gained traction [4,5]. For instance, environmental conditions such as biological growth can markedly reduce resistivity, as observed in coastal concretes exposed to algae and moss [6]. Conversely, introducing calcite-precipitating bacteria has been shown to

improve concrete durability under sulfate exposure [7]. Accordingly, understanding the factors influencing durability parameters and their relative impact is crucial. Measuring the electrical conductivity (or its inverse, resistivity) of concrete is among the most informative durability tests, as it provides insight into a wide range of concrete properties and characteristics [8–11]. However, different test methods can yield varying resistivity values; accordingly, researchers have developed correlations between these methods to ensure consistency in durability evaluation [12]. In recent years, this measurement has gained even greater prominence as a rapid, non-destructive indicator of concrete quality and service life. As demonstrated by Akhondi et al. [13], resistivity measurements directly reflect changes in pore structure when recycled PET and silica fume are incorporated. Researchers have documented strong correlations between a concrete's resistivity and its resistance to processes such as chloride ion penetration and reinforcing steel corrosion [8, 14]. Recent studies have further demonstrated that raising concrete resistivity directly reduces the risk of steel corrosion, confirming resistivity as a reliable indicator of durability [15]. This effect is even more pronounced in air-entrained mixes treated with microbial agents, which exhibited significantly higher resistivity and lower chloride penetrability [16]. As a result, standard test methods (e.g., surface resistivity per AASHTO T358) have been adopted in practice, and resistivity or the related formation factor is increasingly included in performance-based specifications for durability [14,17]. The formation factor, defined as the ratio of a concrete's bulk resistivity to its pore solution resistivity, quantitatively reflects the pore network connectivity; a higher formation factor (and thus higher resistivity) indicates a less connected pore structure and improved durability [14,17]. Notably, the newest performance-based specifications (e.g., AASHTO PP84-17) have recognized this by including the saturated formation factor as a parameter for qualifying concrete's resistance to chloride ingress [17].

One of the earliest theoretical efforts to describe the behavior of composite materials was made in the 19th century by James Clerk Maxwell, who developed an equation relating the electrical conductivity of a two-phase composite to the conductivities of its constituents and their volumetric proportions [18]. Maxwell introduced the concept of a shape factor to account for the influence of inclusion geometry on conductivity. Later, Rayleigh studied Maxwell's shape factor and concluded that Maxwell's formulation underestimated the effect at low volume fractions of inclusions [19]. Slavinski subsequently addressed limitations in the Maxwell and Fricke models, deriving relationships between the shape factor and the relative volume of the conductive phase (paste) for both interconnected and dispersed inclusion scenarios [20].

In 1942, Archie, in his studies on saturated porous sandstones, empirically established a relationship between the bulk electrical resistivity of a rock, its porosity, and the resistivity of the saturating fluid [21]. By introducing a cementation exponent, m (often referred to as the resistivity shape factor), Archie's Law relates rock resistivity to pore geometry and fluid saturation. According to Pearson's 1947 analysis of reservoir data, the exponent m typically ranges from 1.3 for weakly consolidated materials to about 2.2 for well-consolidated materials, serving as an indicator of pore structure and tortuosity [22]. In 1952, Winsauer et al. extended Archie's work to granular mixes of different particle sizes, introducing another empirical constant A (often denoted as the tortuosity factor) to improve the fit for varied grain size distributions [23].

Further refinements to these relationships followed in subsequent decades. Atkins and Smith (1961) applied Archie's Law to each fraction of a multi-component granular system and derived a new combined relationship for the formation factor of the mixture [24]. In 1978, Jackson and colleagues computed A and m for unconsolidated marine sands, extending Archie's formulation and demonstrating how particle shape and packing affect the resistivity–porosity relationship [25]. Keller later noted that Archie's Law is purely empirical and not derived from first principles, compiling extensive ranges of m and A values for various rock types, grain geometries, and porosities, illustrating the law's dependence on material-specific factors [26].

The application of these concepts to cement-based materials began in the late 20th century. Whittington et al. (1981) conducted laboratory studies on mortar and concrete, comparing measured shape factors with values predicted by Maxwell, Fricke, and Slavinski's formulations [27]. They found that the shape factor predictions of Fricke and Slavinski were more consistent with experimental results than Maxwell's, highlighting the importance of accounting for aggregate geometry and distribution. Using an extended form of Archie's Law for concrete (treating the cement paste as the conductive medium and aggregates as inert inclusions), Whittington et al. calculated m and A for various mixes and reported values around $A \approx 1.04$ and $m \approx 1.20$, with a high correlation to measured conductivity [27]. A few years later, Morley and Ford (1987) studied concrete with a 0.5 water–cement ratio over ages ranging from 1 to 65 days and found that $A \approx 1.0$ and $m \approx 1.73$ were needed to fit Archie's Law to their data [28].

More recent research has continued to refine our understanding of Archie's Law in concrete and to address its limitations when applied to a hydrating, multi-phase material. For instance, Glover and colleagues presented a generalized form of Archie's Law that can accommodate any number of phases [29]. This generalized formulation allows for partially conductive solid

phases, acknowledging that in concrete, the cement paste (even when hardened) can conduct charge through pore networks, and that aggregates are not perfectly insulating in all cases. Rangelov and Nassiri empirically characterized the time-dependent evolution of the cement paste's tortuosity in mortar mixes, effectively showing how Archie's cementation exponent m changes as hydration progresses [30]. Their results demonstrated that the classical assumption of constant m (and A) may not hold for concrete at different curing ages—an observation that aligns with experimental findings, which show that the "shape factor" of concrete's microstructure can increase significantly at later ages as continued hydration refines the pore structure [30]. In practical terms, this means that the resistivity of a given concrete mix can rise over time, not just due to reduced pore moisture, but also because the connectivity of the pore network diminishes as the microstructure densifies. Modern studies have also examined the influence of aggregate type and volume on concrete resistivity. Aggregates can interrupt or lengthen the conductive pathways through the paste; accordingly, concrete made with certain aggregate types or with higher aggregate content has shown systematically different resistivity values under identical paste conditions [31]. Such effects underscore the need to account for the shape, size, and distribution of aggregates (i.e., the geometric factors) when predicting concrete's conductivity.

In summary, electrical resistivity testing has evolved into a fundamental tool for evaluating concrete durability. Contemporary research and standards reflect this evolution: strong correlations have been established between resistivity (or formation factor) and durability metrics, and improved models based on Archie's Law have been developed to better represent the composite nature of concrete. In this study, an extended form of Archie's Law, combined with a shape factor approach, is employed to evaluate the electrical conductivity of concrete, with the cement paste serving as the primary conductive phase. A comprehensive experimental program was designed involving 80 concrete mix designs prepared by varying key parameters such as aggregate type (marble and tuff), grading (Fuller curve exponents from 0.2 to 0.65), maximum aggregate size (9.5 mm and 19 mm), and relative volume of cement paste (0.25 to 0.45). Specimens were cured and tested at multiple ages (3, 7, 28, and 150 days) to examine time-dependent effects. Measurements included both the bulk electrical conductivity of concrete and the resistivity of aggregates, using a custom experimental setup designed to enhance accuracy.

The study focuses on evaluating how changes in mixture composition and curing age affect the parameters m and A in the modified Archie model. The objective is to assess the model's predictive capacity across different microstructural configurations and to identify its limitations

over time. This approach enables a more rigorous understanding of conductivity mechanisms in cement-based materials, with implications for durability-based concrete design.

2. MATERIALS AND METHODS

In this study, samples were prepared to examine shape factor theories, with the cement paste serving as the conductive phase.

2.1. Relative Volume of Cement Paste in Concrete

The relative volume of cement paste in conventional concrete typically ranges from 0.3 to 0.4. However, to achieve a more detailed analysis of this parameter, the range of 0.25 to 0.45 was selected for this research. Due to the absence of superplasticizers and the replacement of 7.5% of the cement with microsilica pozzolan, mixes with a relative cement paste volume below 0.25 were very coarse and difficult to place into moulds. Similarly, using a relative cement paste volume greater than 0.45 is uncommon in concrete mixes.

2.2.Maximum Aggregate Size

Since the findings of this study are primarily relevant to marine structures and corrosion issues, where maximum aggregate sizes are generally smaller than those used in other reinforced concrete structures, a maximum aggregate size of 19 mm was chosen as the upper limit for this parameter. Conversely, aggregates with a maximum size smaller than 9.5 mm are rarely used in structures, making this value the lower limit of this parameter's range.

Given the relatively lower importance of this parameter compared to other factors, selecting values between 9.5 and 19 mm was deemed unnecessary. By applying these values to the concrete mix, concretes with electrical resistivity ranging from very low to very high were achieved.

Table 1.
Variables considered in the concrete mix designs

Row	Aggregate Type	Curing Age (days)	Relative Cement Paste Volume	Curve Power	Maximum Aggregate Size (mm)
1	Marble	3	0.25	0.2	9.5
2	Tuff	7	0.3	0.35	19
3	-	28	0.35	0.5	-
4	-	150	0.4	0.65	-
5	-	-	0.45	-	-

2.3.Water

For the mixtures in this research, where the mineral content of the water had no significant role,

potable water was used.

2.4.Cement

In the mix designs used in this study, no specific properties of the cement were considered. Ordinary Portland cement (Type I) produced by Sepahan Cement Factory in Isfahan was used, and its physical and chemical properties, as determined by the factory's laboratory results, are presented in Table 2. Additionally, the density of the cement was measured according to ASTM C188-03 [32] and reported as 3180 kg/m³.

Table 2.

Physical and chemical properties of type I cement from Sepahan factory.

Physical Properties												
Specific Surface Area (m^2/kg)	Initial Setting Time (min)	Final Setting Time (min)	CaO	SiO_2	Al_2O_3	Fe_2O_3	MgO	SO_3	Free CaO	LOI	Eq. alkalis	IR
330	190	240	63.5	21.5	5.3	3.3	2.4	2	1	0.8	0.75	0.4

2.5.Micro-silica

Microsilica, a by-product of the ferrosilicon and ferroalloy industries, exhibits exceptionally high pozzolanic properties. In this study, microsilica produced by the Azna factory was used due to its high quality. The chemical analysis and physical properties of this pozzolan, as determined by the laboratory results of the mentioned factory, are presented in Table 3.

Table 3.

Chemical and physical properties of microsilica from Azna factory.

Physical Properties	**Chemical Properties**												
Specific Surface Area (m^2/kg)	SO_3	P_2O_3	Carbon (C)	Na_2O	CaO	Silicon carbide (SiC)	Moisture (H_2O)	Fe_2O_3	MgO	K_2O	Chloride (Cl)	Al_2O_3	SiO_2
1400	0.1	0.16	0.3	0.31	0.49	0.5	0.8	0.87	0.97	1.01	1.04	1.32	94.6-96.4

2.6. Aggregates

In the mix designs of this study, two types of aggregates with metamorphic and volcanic origins were used. Marble aggregates with a metamorphic origin were sourced from the Alvan mine in Yazd, while tuff aggregates with a volcanic origin were extracted from the Sabz mine in Qom (Fig. 1). To achieve different Fuller-Thompson curve gradations, all aggregates were sieved using standard sieves in accordance with ASTM C136-01 [33]. Additionally, tests for

188 determining relative density and water absorption were performed on each aggregate size
189 following the ASTM C127-01 [34] and ASTM C128-01 [35] standards.

190 **Table 4.**

191 Results of water absorption and relative density of marble aggregate.

Size (mm)	19	9.5	4.75	2.36	1.19	0.6	0.3	0.15
Relative density (saturated surface-dry, g/cm³)	2.57	2.55	2.61	2.66	2.63	2.64	2.59	2.71
Relative density (oven-dried, g/cm³)	2.52	2.51	2.54	2.59	2.55	2.57	2.54	-
Water absorption (%)	0.2	1.9	2.9	2.6	3.4	2.6	2.2	-

192

193 **Table 5.**

194 Results of water absorption and relative density of tuff aggregate.

Size (mm)	19	9.5	4.75	2.36	1.19	0.6	0.3	0.15
Relative Density (saturated surface-dry, g/cm³)	2.31	2.34	2.39	2.38	2.4	2.39	2.41	2.59
Relative Density (oven-dried, g/cm³)	2.19	2.19	2.23	2.23	2.26	2.25	2.3	-
Water Absorption (%)	5.2	6.8	7.1	6.7	6.2	6.2	5.8	-

195 **Fig. 1.** Gradation curve of aggregate mixture

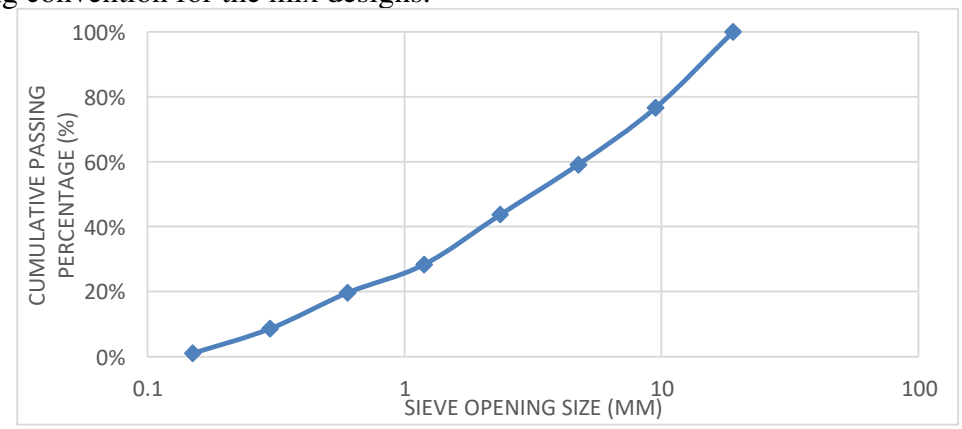
196 **2.7. Mix Design Presentation and Test Arrangement**

197 The naming convention for the mix designs is shown in Table 6.

198

199 **Table 6.**

200 Naming convention for the mix designs.



Index number	Relative volume of cement paste	Curve power	Type of aggregate	Maximum aggregate size (mm)
1	0.45	0.65	Marble	19
2	0.4	0.5	Tuff	9.5
3	0.35	0.35	-	-
4	0.3	0.2	-	-
5	0.25	-	-	-

For example, a mix design with a relative cement paste volume of 0.30, a curve exponent of 0.63, marble aggregate, and a maximum aggregate size of 19 mm is designated as Mix 3112.

Table 7.

Mix designs for concretes with marble aggregate (per 1 m³).

Row	Name	Cement (kg)	Microsilica (kg)	Free water (kg)	Saturated surface-dry aggregate weight (kg)							
					19	9.5	4.75	2.36	1.19	0.6	0.3	0.15
1	1112	476	39	283	0	533	346	225	141	91	57	38
2	2111	423	34	252	574	364	237	154	96	62	39	26
3	3112	371	30	220	0	629	409	266	166	108	68	45
4	4111	318	26	189	670	425	276	180	112	73	46	30
5	5112	265	21	157	0	726	472	307	192	124	78	52
6	1211	476	39	283	441	310	224	162	112	81	56	41
7	2212	423	34	252	0	493	355	257	178	128	89	66
8	3211	371	30	220	522	367	265	191	132	95	66	49
9	4212	318	26	189	0	575	415	299	207	149	104	77
10	5211	265	21	157	602	423	305	221	153	110	76	57
11	1312	476	39	283	0	371	297	238	183	145	112	92
12	2311	423	34	252	388	303	242	194	149	119	92	75
13	3312	371	30	220	0	438	351	281	216	172	133	109
14	4311	318	26	189	452	353	283	226	174	139	107	88
15	5312	265	21	157	0	506	405	324	249	198	153	126
16	1411	476	39	283	273	237	210	187	159	140	120	110
17	2412	423	34	252	0	320	284	252	215	190	163	148
18	3411	371	30	220	323	280	248	221	188	166	142	130
19	4412	318	26	189	0	373	331	294	251	222	190	173
20	5411	265	21	157	372	323	286	255	217	192	164	149

Table 8.

Mix designs for concretes with tuff aggregate (per 1 m³).

Row	Name	Cement (kg)	Microsilica (kg)	Free water (kg)	Saturated surface-dry aggregate weight (kg)							
					19	9.5	4.75	2.36	1.19	0.6	0.3	0.15
1	1122	476	39	283	0	488	317	202	128	83	53	36
2	2121	423	34	252	516	334	217	138	88	57	36	25
3	3122	371	30	220	0	577	375	238	152	98	63	43
4	4121	318	26	189	602	389	253	161	102	66	43	29

5	5122	265	21	157	0	665	432	275	175	113	73	50
6	1221	476	39	283	396	284	205	145	102	73	52	40
7	2222	423	34	252	0	451	325	229	162	116	83	63
8	3221	371	30	220	468	336	242	171	121	86	62	47
9	4222	318	26	189	0	527	380	268	189	135	97	73
10	5221	265	21	157	540	388	280	197	139	100	71	54
11	1322	476	39	283	0	340	272	213	167	132	105	88
12	2321	423	34	252	348	277	222	174	136	108	85	72
13	3322	371	30	220	0	401	321	251	197	156	124	104
14	4321	318	26	189	406	323	259	202	159	126	100	84
15	5322	265	21	157	0	463	370	290	227	180	143	120
16	1421	476	39	283	245	217	192	167	145	128	112	105
17	2422	423	34	252	0	293	260	226	196	173	151	141
18	3421	371	30	220	290	256	227	197	171	151	132	124
19	4422	318	26	189	0	342	303	263	229	201	177	165
20	5421	265	21	157	334	295	262	228	198	174	153	143

Table 9.

Mix proportions for the cement paste (per 1 m³) used across mixes.

Set of mix designs	Cement (kg)	Silica fume (kg)	Water (kg)
	1059	86	629

The number, type, geometry, dimensions, and age of specimens and tests are presented in Table 10.

Table 10.

Number, type, and age of tests, number of specimens, and volume of concrete and cement paste prepared for the first set of mix designs

Tests	Age (days)	Number of specimens per age	Total number of specimens	Type of specimen	Geometry of specimen	Specimen dimensions (mm)
Determination of electrical conductivity	3, 7, 28, and 150	3	3	Concrete	Cylindrical	Diameter 100, Height 200
Determination of electrical conductivity	3, 7, 28, and 150	3	3	Cement paste	Cylindrical	Diameter 100, Height 200
Determination of electrical resistivity	-	2	2	Aggregate	Cylindrical	Diameter 100, Height 200

2.8. Preparation, Molding, and Curing of Laboratory Samples

All stages of concrete preparation, casting, and curing were performed in accordance with ASTM C192-02 [36]. First, the inner surface of the mixer was moistened to prevent water absorption during the mixing process. Then, the coarse aggregates, along with a portion of the

mixing water, were added and mixed. Subsequently, fine aggregates, cement, and the remaining water were gradually added while the mixer was running. If microsilica was used in powder form, it was first dissolved in the mixing water and then added to the mixture.

After all materials were added, the mixing process consisted of three minutes of mixing, followed by a three-minute rest, and a final two minutes of mixing. During the mixing process, the mixer was covered to prevent water evaporation. The prepared concrete was poured into moulds in multiple layers, with each layer compacted using a vibrating table. The concrete surface was leveled with a trowel, and the moulds were covered with plastic to prevent evaporation of surface water. After 24 ± 6 hours, the specimens were demoulded and stored in a lime-saturated water bath for curing.

2.9.Test for Measuring the Electrical Conductivity of Concrete and Cement Paste

The equipment required for this test included two water and salt reservoirs placed on either side of the specimen, a 60-volt DC generator, and an ammeter with an accuracy of 0.1 mA, as shown in Figs. 2 and 3.



Fig. 2. 60-volt DC generator used in the electrical conductivity measurement test



Fig. 3. Ammeter with 0.1 mA accuracy used in the electrical conductivity measurement test

In this method, the specimen is a cylinder with a diameter of 100 mm and a height of 200 mm, and the electrodes are a 3% by weight saltwater solution contained in reservoirs on either side of the specimen. A 60-volt DC voltage is applied to the specimen for 60 seconds, after which the input current is read using an ammeter connected in series within the circuit. Finally, the electrical conductivity is calculated using Ohm's Law, simplified as Equation (1):

$$\sigma = K \cdot \frac{I_1}{V} \cdot \frac{L}{D^2} \quad (1)$$

In this method, the bulk electrical conductivity (σ) is calculated in milli-Siemens per meter (mS/m). The current passing through the specimen (I_1) is measured in milliamps (mA), while the applied voltage (V) is in volts (V). The average length of the specimen (L) is measured in millimeters (mm), and the average diameter of the specimen (D) is also in millimeters (mm). The conversion factor (K) is 1273.2 (for cylinders with a diameter of 100 mm and a height of 200 mm). These values are used in the formula provided to calculate the electrical conductivity.

2.10. Measurement of Electrical Resistivity of Aggregates

In this study, an innovative method was introduced to measure the electrical resistivity of aggregates, addressing the limitations of the four-electrode method. In this approach, saturated surface-dry aggregates are compacted at a specific density within a polyethylene mold (100 mm in diameter and 200 mm in height), and their apparent electrical resistance is measured using a spectrometer.

For preparation, the weight of the aggregates is calculated based on their bulk and relative densities, and the aggregates are compacted in the mold. After compaction using a vibrating table, the sample surface is coated with a layer of fresh cement paste, and the apparent electrical resistance is recorded at the smallest phase difference between voltage and current. The electrical resistivity is then calculated using the following equations:

$$R = Z \cdot \cos\varphi \quad (2)$$

where, R is the electrical resistance in ohms (Ω), Z is the apparent electrical resistance in ohms (Ω), and φ is the phase difference between voltage and current in degrees.

$$\rho = \frac{R \cdot A}{L} \quad (3)$$

where:

- ρ = electrical resistivity
- R = resistance
- A = cross-sectional area
- L = sample length

This method enables the measurement of the resistivity of aggregates with different gradations and types and is more cost-effective compared to the four-electrode method. Other studies have shown that reducing aggregate porosity, such as by microbial calcium carbonate treatment, can further increase bulk resistivity [37].

3. Results and Discussion

3.1. Evaluation of the Extended Archie's Model (Shape Factor Approach)

The extended Archie's law, within the framework of the shape factor approach, is the primary and most common expression for describing the mechanism of composite materials in conducting electrical current. In this study, this model is the focus, and the constants A and m are examined, with the fundamental assumptions of this approach being analyzed for concrete. Since the core assumption in the shape factor approach is the infinite ratio of $\frac{\rho_A}{\rho_p}$, the parameters ρ_A and v_A are selected to study the behavior of constants A and m. To this end, the behavior of parameter A against variations in ρ_A and v_A is investigated across all samples. Due to the similar behavior observed, for example, the results of 20 mix designs with marble aggregates at a 3-day age are presented in Figs. 4 and 5.

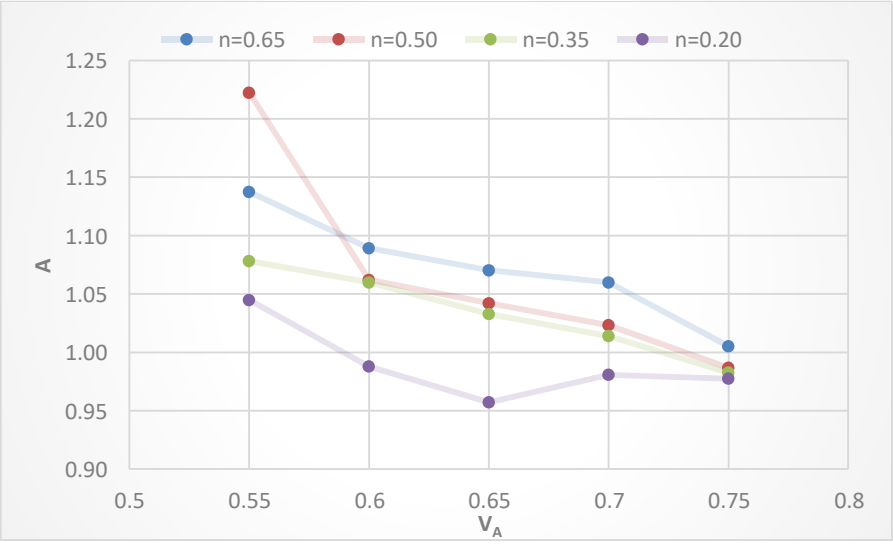


Fig. 4. Variations in parameter a with changes in v_A for first 20 mix designs with marble

aggregates at 3-day age using the extended Archie's model

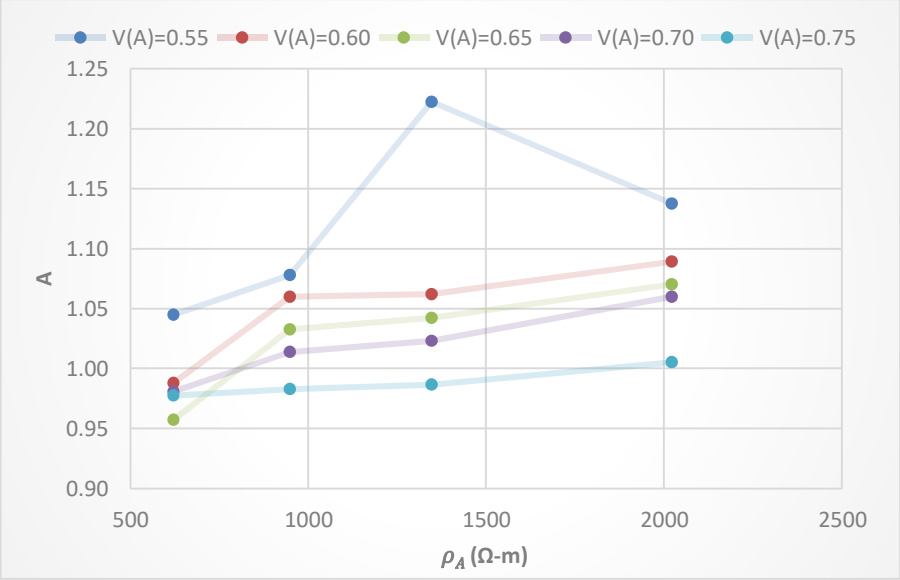


Fig. 5. Variations in parameter A with changes in ρ_A for first 20 Mix designs with marble aggregates at 3-day age using extended Archie's model

Based on the laboratory results, as v_A increases, parameter A decreases, and as ρ_A increases, parameter A increases. To examine the simultaneous effect of ρ_A and v_A, the changes in parameter A with the ratio $\frac{\rho_c}{\rho_p}$ are shown in all measurements in Fig. 6.

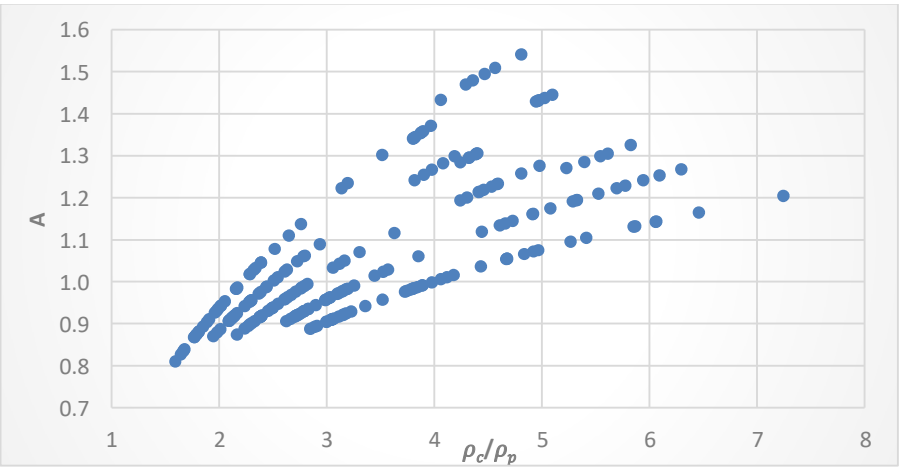


Fig. 6. Variations in parameter A with changes in $\frac{\rho_c}{\rho_p}$ for all measurements in the extended Archie's model

Based on the laboratory results, as $\frac{\rho_c}{\rho_p}$ increases, parameter A increases, and in the limiting case, its change approaches zero. The existence of such behavior indicates the dominant effect of

ρ_A on parameter A, which aligns meaningfully with the fundamental assumption of the shape factor approach. In Fig. 6, each set of points located on a curve corresponds to a specific volume of cement paste. The highest set is associated with a relative cement paste volume of 0.45, and this value gradually decreases from top to bottom to 0.40, 0.35, 0.30, and 0.25, respectively. Therefore, as ρ_A increases, parameter A in each relative cement paste volume tends toward a specific value, which is consistent with the basis of the extended Archie's law. Parameter m also shows similar behavior to A, as shown in Figs. 7 to 9.

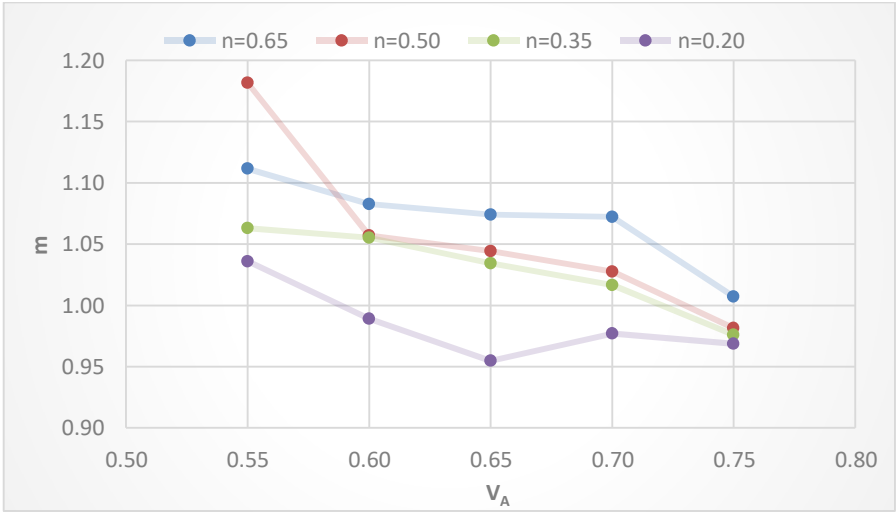


Fig. 7. Variations in parameter m with changes in v_A for first 20 mix designs of marble aggregate at 3 days in the extended Archie' model

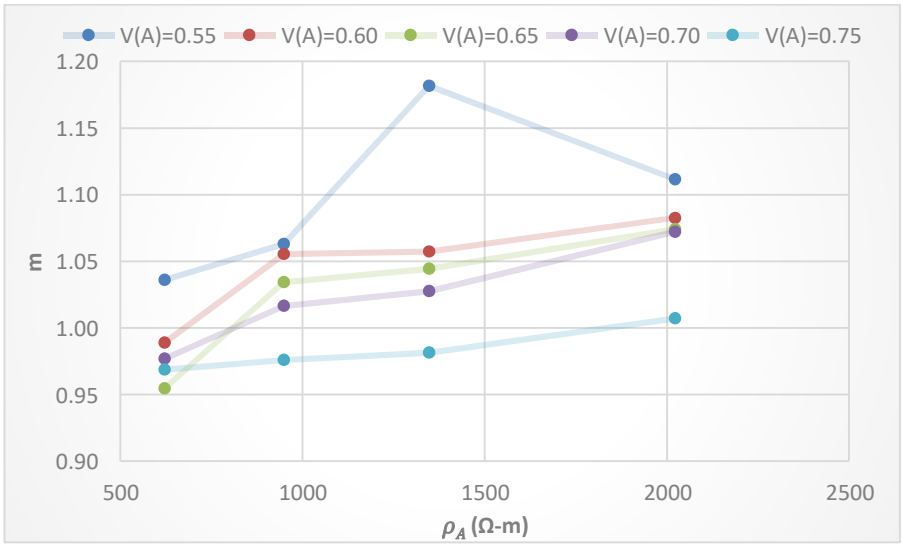


Fig. 8. Variations in parameter *m* with changes in ρ_A for first 20 mix designs of marble aggregate at 3 days in the extended Archie's model

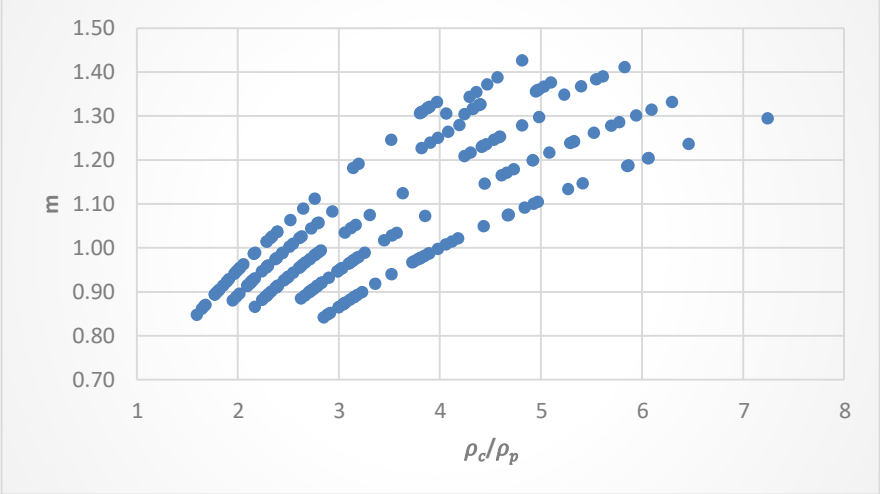


Fig. 9. Variations of parameter *m* with changes in $\frac{\rho_c}{\rho_p}$ across all measurements

Thus, the higher the value of $\frac{\rho_c}{\rho_p}$, the more accurate the shape factor approach will be in describing the behavior of concrete. The average values of parameters A and m in all measurements are 1.538 and 1.532, respectively. However, the correlation coefficient of the developed Archie's law with the calculated values of A and m in this study is very low, and it is not possible to predict ρ_c with adequate accuracy. It is worth noting that the range of variation for parameter A is between 1.809 and 1.5403, and the range for parameter mmm is between 1.8413 and 1.4264. The values obtained for A and m are similar to those reported by Whittington and colleagues, as well as Morley and Ford. Mixes with tuff aggregate exhibited lower bulk conductivity than marble mixes under identical conditions, reflecting the influence of aggregate mineralogy and internal pore structure.

Additionally, another fundamental assumption of the developed Archie's law is the invariance of the shape factor over time (curing age). This has been examined in all the samples, and due to the similarity, the results for the first five mixes of marble aggregate at ages 3, 7, and 28

days are shown in Fig. 10, and for the tuff aggregate in Fig. 11.

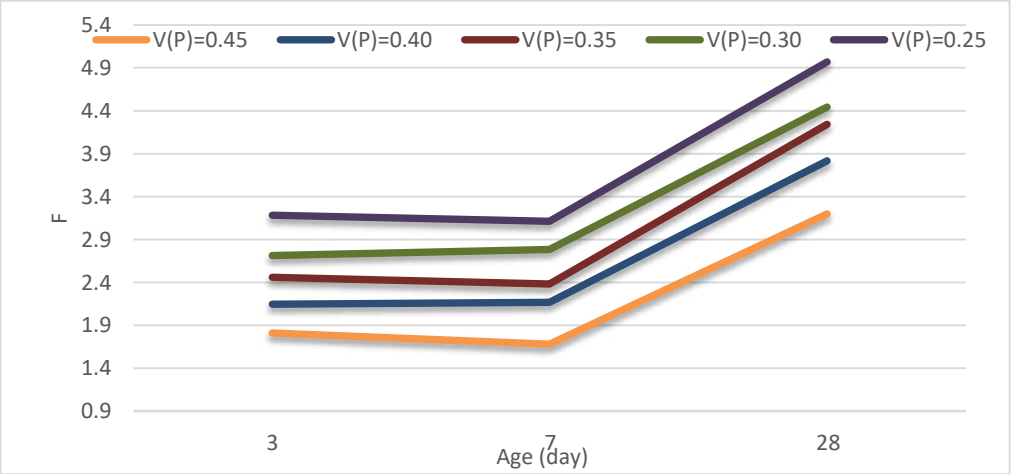


Fig. 10. Changes in shape factor with changes in curing age for first five mix designs using marble aggregate

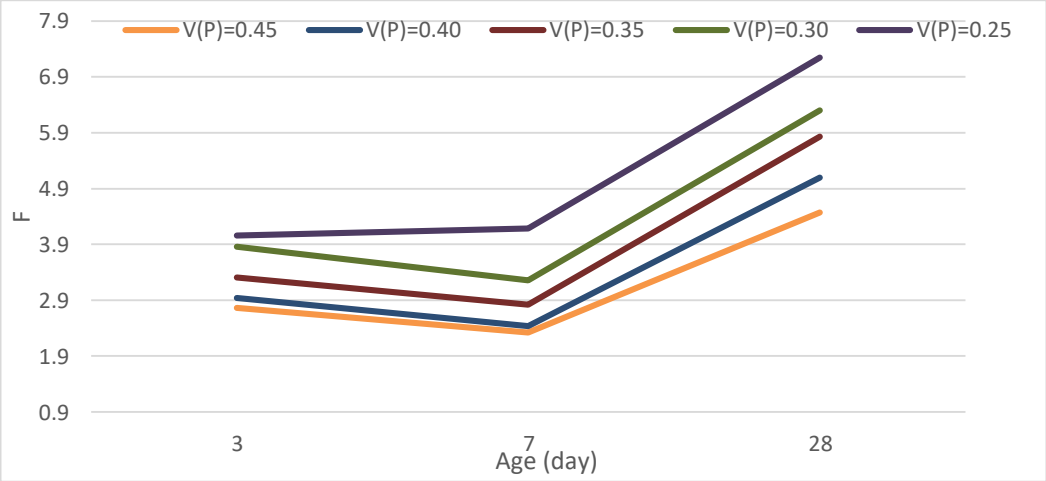


Fig. 11. Changes in shape factor with changes in curing age for \ first five mix designs using tuff aggregate

One of the critical findings of this research is the significant variation in the parameters A and m over time, which is closely linked to the evolving microstructure of the cement paste. As hydration progresses, the volume of unreacted cement decreases, and the pore structure becomes increasingly segmented. In particular, the interfacial transition zone (ITZ), especially in mixtures with finer aggregates or higher cement paste content, becomes denser and less porous. This densification reduces ionic mobility and contributes to the observed increase in the parameter m, reflecting more tortuous and complex conductive pathways. These observations are consistent with the findings of Rangelov and Nassiri [24], who reported an association between increased tortuosity and extended curing durations.

The continuous decline observed in parameter A over time can also be explained by the redistribution of ionic species in the pore solution and the reduction in the diameter of capillary pores. At early ages, high ionic concentrations and the presence of wide, continuous capillary pores promote electrical conductivity, resulting in higher A values. As hydration advances, the formation of hydration products lowers the conductivity of the pore solution, and conduction shifts toward narrower gel pores that offer higher resistance. This transition results in a noticeable decline in electrical conductivity, highlighting a key limitation of Archie's original model, which assumes constant values for A and m regardless of the evolving material structure. This behavior is also linked to changes in the structure and thickness of the transition layer between the cement paste and the aggregates. It is likely that at later ages, either the electrical resistivity of the ITZ itself increases or the microstructural transformations within this zone reduce its ability to facilitate ionic transport. In either case, the interaction between the maturing paste and the surrounding aggregates significantly alters the global resistivity of the concrete matrix.

A key distinction between the findings of this study and earlier models is the explicit time dependence observed in the parameters A and m, which were initially assumed to be constant in traditional Archie-based approaches [27, 28]. While Whittington et al. and Morley and Ford reported relatively fixed values for A and m under limited mix and age conditions, our data demonstrate clear temporal evolution in both parameters across diverse mix designs and curing intervals. This divergence highlights the importance of considering microstructural transformations during hydration, particularly the densification of the paste matrix and changes in the interfacial transition zone. The evolving values of A and m observed in this study suggest that a static calibration of these parameters is insufficient for long-term modeling, especially in concretes with significant variation in paste volume or aggregate morphology.

Moreover, the role of mixture design on electrical conductivity was found to be more pronounced than previously indicated in the literature. For example, mixes with higher cement paste volume showed elevated conductivity not only at early ages, due to ionic-rich pore solutions, but also at later ages, likely due to more connected gel pore networks. This dual-stage conductivity behavior challenges the binary conductive/non-conductive interpretation used in simplified formation factor models, pointing to a more complex, time-sensitive mechanism. Similarly, Dousti (2022) reported that mortars containing calcined clays exhibited refined pore structures and significantly higher electrical resistivity, confirming the strong link between microstructural modification and durability performance [38]. These findings reinforce the need for updated durability modeling frameworks that integrate time-evolving

microstructure, aggregate resistivity, and the changing nature of pore solution conductivity to more accurately predict service life behavior in real-world structures.

4. CONCLUSION

This research investigated the electrical conductivity of concrete using an extended Archie's model that incorporates aggregate shape factors and considers the cement paste as the primary conductive phase. Based on testing 80 concrete mixes with varying aggregate type, gradation, maximum size, and cement paste volume over 3, 7, 28, and 150 days, the following key findings were identified:

1. Model Accuracy at Early Ages: The extended Archie's law provided highly accurate predictions of electrical conductivity at early curing stages, with a correlation coefficient of $R \approx 0.97$ at 3–7 days, significantly outperforming conventional approaches.
2. Time-Dependent Parameters: The model parameters A (tortuosity factor) and m (cementation exponent) exhibited apparent age-related variation:

- A decrease from 1.81 at 3 days to 1.54 at 150 days (~15% reduction),
- m increased from 1.43 to 1.84 over the same period (~29% increase),

indicating an increase in microstructural tortuosity and densification over time.

3. Effect of Cement Paste Volume: Electrical conductivity increased consistently with cement paste volume. The highest conductivity was observed at a paste volume of 0.45, confirming the significant role of the paste fraction in facilitating ionic transport.
4. Aggregate Type and Resistivity: Tuff aggregates, having higher porosity and water absorption, contributed to lower bulk conductivity compared to marble aggregates under similar mix designs, underscoring the effect of aggregate mineralogy and electrical resistivity.
5. Model Limitations at Later Ages: The evolving pore network and changes in the interfacial transition zone (ITZ) reduced the model's predictive capacity beyond 28 days. The assumption of time-invariant parameters A and m becomes invalid at advanced hydration stages, limiting long-term applicability without recalibration.

These results confirm that accounting for aggregate geometry, cement paste volume, and curing age is essential in conductivity-based durability modeling. The observed time-dependence of key parameters suggests that future models should incorporate dynamic calibration to improve long-term prediction accuracy.

Acknowledgments:

Not applicable. The authors received no financial support and have no additional acknowledgments to declare.

Conflict of Interest

The authors declare that they have no known competing financial interests or personal relationships that could have appeared to influence the work reported in this paper.

Data Availability

The data that support the findings of this study are available from the corresponding author upon reasonable request.

Supplementary Information:

Not applicable.

Ethical Approval

Not applicable. This study did not involve human participants or animal experiments.

Clinical trial number: not applicable.

Consent to participate: not applicable.

Consent to publish: not applicable.

REFERENCES

1- P. Azarsa, R. Gupta, Electrical resistivity of concrete for durability evaluation: A review, Adv. Mater. Sci. Eng. (2017) 8453095, 1-30. https://doi.org/10.1155/2017/8453095

2- N.S. Piro, A.S. Mohammed, S.M. Hamad, Electrical resistivity measurement, piezoresistivity behavior and compressive strength of concrete: A comprehensive review, Mater. Today Commun. (2023) 106573, 123-132. https://doi.org/10.1016/j.mtcomm.2023.106573

3- A.A. Kafash Bazari, M. Chini, Laboratory evaluation of electrical resistance of concrete, J. Civil Eng. Mater. Appl. 6(2) (2022) 99–111. 10.22034/jcema.2022.333341.1082

4- D. Qin, P. Gao, F. Aslam, M. Sufian, H. Alabduljabbar, A comprehensive review on fire damage assessment of reinforced concrete structures, Case Stud. Constr. Mater. 16 (2022) e00843, https://doi.org/10.1016/j.cscm.2022.e00843

5- H. Yang, L. Liu, W. Yang, et al., A comprehensive overview of geopolymer composites: A bibliometric analysis and literature review, Case Stud. Constr. Mater. 16 (2022) e00830, https://doi.org/10.1016/j.cscm.2022.e00830

6- S. Bozorgmehr Nia, R. Jamalpour, M. Taheri, Assessing the durability of coastal high-performance concrete (HPC) structures exposed to biodegradables such as algae and moss, J. Civil Eng. Mater. Appl. 7(2) (2023) 121–129 https://doi.org/10.22034/jcema.2023.406793.1115

7- F. Nosouhian, D. Mostofinejad, H. Hasheminejad, Concrete durability improvement in a sulfate environment using bacteria, J. Mater. Civ. Eng. 28(1) (2016) 04015064. https://doi.org/10.1061/(ASCE)MT.1943-5533.0001382

8- H. Layssi, P. Ghods, A.R. Alizadeh, M. Salehi, Electrical resistivity of concrete, Concr. Int. 37(5) (2015) 41–46.

9- G. Cosoli, A. Mobili, F. Tittarelli, G.M. Revel, P. Chiariotti, Electrical resistivity and electrical impedance measurement in mortar and concrete elements: A systematic review, Appl. Sci. 10(24) (2020) 9152, https://doi.org/10.3390/app10249152

10- O.E. Gjørv, Durability of concrete structures, Arab. J. Sci. Eng. 36 (2011) 151–172.

11- H. Beushausen, R. Torrent, M.G. Alexander, Performance-based approaches for concrete durability: State of the art and future research needs, Cem. Concr. Res. 119 (2019) 11–20.

12- Parsian, H., Tadayon, M., Mostofinejad, D., & Avatefi, F. (2018). Experimental Study on Correlation between Resistivity Measurement Methods in Concrete. ACI Materials Journal, 115(1), 33-45.

13- M. Akhondi, T. Pour Rostam, A. Golsorat Pahlaviani, Synergistic effects of recycled PET particles and silica fume on the fresh, hardened and durability performance of roller compacted concrete, J. Civil Eng. Mater. Appl. 7(4) (2023) 243–257, https://doi.org/10.22034/jcema.2024.433811.1129

14- J.C. Maxwell, A Treatise on Electricity and Magnetism, vol. 1, Clarendon Press, Oxford, UK (1873), https://www.loc.gov/item/03015568/

15- B. Tayebani, D. Mostofinejad, Penetrability, corrosion potential, and electrical resistivity of bacterial concrete, J. Mater. Civ. Eng. 31(3) (2019) 04019002, https://doi.org/10.1061/(ASCE)MT.1943-5533.0002639

16- N. Parastegari, D. Mostofinejad, D. Poursina, Use of bacteria to improve electrical resistivity and chloride penetration of air-entrained concrete, Constr. Build. Mater. 210 (2019) 588–595,

https://doi.org/10.1016/j.conbuildmat.2019.03.216

17- L. Rayleigh, On the influence of obstacles arranged in rectangular order upon the properties of a medium, Philos. Mag. 34 (1892) 481–502.

https://doi.org/10.1080/14786449208620364

18- A. Slawinski, Conductivity of an electrolyte containing dielectric bodies, J. Chem. Phys. 23 (1926) 710–713.

19- G.E. Archie, The electrical resistivity log as an aid in determining some reservoir characteristics, Trans. AIME 146 (1942) 54–62.

20- S.J. Pirson, Electric logging factors which affect true formation resistivities, Oil Gas J. 46(26) (1947) 76–81.

21- W.O. Winsauer, H.M. Shearin, P.H. Masson, M. Williams, Resistivity of brine-saturated sands in relation to pore geometry, AAPG Bull. 36(2) (1952) 253–277.

22- E.R. Atkins, G.H. Smith, The significance of particle shape in formation resistivity factor–porosity relationships, J. Pet. Technol. 222 (1961) 285–291.

23- P.D. Jackson, D. Taylor Smith, P.N. Stanford, Resistivity–porosity–particle shape relationships for marine sands, Geophysics 43(6) (1978) 1250–1268.

24- G.V. Keller, Electrical properties of rocks and minerals, in: Handbook of Physical Properties of Rocks, Vol. 1, CRC Press, Boca Raton, FL, USA (1982) 217–293.

25- H.W. Whittington, W.J. McCarter, M.C. Forde, The conduction of electricity through concrete, Mag. Concr. Res. 33(114) (1981) 48–60, https://doi.org/10.1680/macr.1981.33.114.48

26- C.T. Morley, M.C. Ford, Electrical conduction through concrete using formation factor theories, in: Proc. International Conference on Structural Faults and Repair, London, UK (1987) 411–422.

27- P.W.J. Glover, A generalized Archie's law for n phases, Geophysics 75(6) (2010) E247–E265.

28- M. Rangelov, S. Nassiri, Empirical time-dependent tortuosity relations for hydrating mortar mixtures based on modified Archie's law, Constr. Build. Mater. 171 (2018) 825–838.

29- C. Qiao, M.K. Moradllo, H. Hall, M.T. Ley, W.J. Weiss, Electrical resistivity and formation factor of air-entrained concrete, ACI Mater. J. 116(3) (2019) 85–94.

30- K.P.V. Robles, J.J. Yee, S.-H. Kee, Electrical resistivity measurements for nondestructive evaluation of chloride-induced deterioration of reinforced concrete: A review, Materials 15(8) (2022) 2725, https://doi.org/10.3390/ma15082725

31- AASHTO PP84-17, Standard Practice for Developing Performance Engineered Concrete Pavement Mixtures, AASHTO, Washington, DC (2017).

531 32- ASTM C188-95, Standard Test Method for Density of Hydraulic Cement, ASTM
532 International (2003), https://doi.org/10.1520/C0188-95R03

533 33- ASTM C136-01, Standard Test Method for Sieve Analysis of Fine and Coarse
534 Aggregates, ASTM International (2001), https://doi.org/10.1520/C0136-01

535 34- ASTM C127-01, Standard Test Method for Density, Relative Density (Specific
536 Gravity), and Absorption of Coarse Aggregate, ASTM International (2001),
537 https://doi.org/10.1520/C0127-01

538 35- ASTM C128-01, Standard Test Method for Density, Relative Density (Specific
539 Gravity), and Absorption of Fine Aggregate, ASTM International (2001),
540 https://doi.org/10.1520/C0128-01

541 36- ASTM C192/C192M-02, Standard Practice for Making and Curing Concrete Test
542 Specimens in the Laboratory, ASTM International (2002),
543 https://doi.org/10.1520/C0192_C0192M-02

544 37- N.H. Balam, D. Mostofinejad, M. Eftekhar, Effects of bacterial remediation on
545 compressive strength, water absorption, and chloride permeability of lightweight
546 aggregate concrete, Constr. Build. Mater. 145 (2017) 107–116,

547 https://doi.org/10.1016/j.conbuildmat.2017.03.211

548 38- Dousti, A., Beyki, H., & Shekarchi, M. (2022). Strength and durability performance of
549 mortars incorporating calcined clay as pozzolan in comparison with silica fume. Journal
550 of Civil Engineering and Materials Application, 6(3), 159-174.

551 https://doi.org/10.22034/jcema.2022.361685.1096

552

553